An Elevated Level of Cholesterol Impairs Self-Assembly of Pulmonary Surfactant into a Functional Film

Zoya Leonenko,* Simardeep Gill,* Svetlana Baoukina,† Luca Monticelli,† Jana Doehner,* Lasantha Gunasekara,* Florian Felderer,* Mathias Rodenstein,‡ Lukas M. Eng,‡ and Matthias Amrein*

*Department of Cell Biology and Anatomy, Faculty of Medicine, and †Department of Biological Sciences, Faculty of Science, University of Calgary, Calgary, Alberta, Canada; and ‡Institute of Applied Photophysics, University of Technology Dresden, Dresden, Germany

ABSTRACT In adult respiratory distress syndrome, the primary function of pulmonary surfactant to strongly reduce the surface tension of the air-alveolar interface is impaired, resulting in diminished lung compliance, a decreased lung volume, and severe hypoxemia. Dysfunction coincides with an increased level of cholesterol in surfactant which on its own or together with other factors causes surfactant failure. In the current study, we investigated by atomic force microscopy and Kelvin-probe force microscopy how the increased level of cholesterol disrupts the assembly of an efficient film. Functional surfactant films underwent a monolayer-bilayer conversion upon contraction and resulted in a film with lipid bilayer stacks, scattered over a lipid monolayer. Large stacks were at positive electrical potential, small stacks at negative potential with respect to the surrounding monolayer areas. Dysfunctional films formed only few stacks. The surface potential of the occasional stacks was also not different from the surrounding monolayer. Based on film topology and potential distribution, we propose a mechanism for formation of stacked bilayer patches whereby the helical surfactant-associated protein SP-C becomes inserted into the bilayers with defined polarity. We discuss the functional role of the stacks as mechanically reinforcing elements and how an elevated level of cholesterol inhibits the formation of the stacks. This offers a simple biophysical explanation for surfactant inhibition in adult respiratory distress syndrome and possible targets for treatment.

INTRODUCTION

Lung compliance is dominated by the surface tension of the hydration layer covering the lung epithelium to the air (1). The air-water interface is covered by a tightly packed molecular film of pulmonary surfactant. The film hinders the interface from contracting under the influence of the surface tension. It thus reduces the surface tension from ~72 mN/m of a bare air-water interface to <1 mN/m once the air-lung interface is at its minimum size at end expiration (2). The surface tension likely always remains <10 mN/m during tidal breathing in the healthy lung (3). A low surface tension is required to reduce the Laplace pressure, which otherwise would cause the alveoli to collapse into the small airways.

In adult respiratory distress syndrome (ARDS), pulmonary surfactant function is inhibited. As a result, the surface tension is elevated and the lung function substantially impaired. ARDS is a common and devastating condition with 150,000 cases per year in the US and a mortality rate of ~30%. Because surfactant impairment is likely a major factor for the morbidity and mortality of ARDS, it has been targeted by replacement surfactant therapy. However, success has been minimal (for a review, see (4)) because the exogenous surfactant apparently also became inactivated. A better understanding of the cause and mechanism of the inactivation may therefore be required to counter it more specifically.

Until recently, surfactant inhibition in ARDS has been investigated mainly with regard to serum proteins, which are highly elevated in the alveolar space in the case of ARDS (e.g., (4–6)) and oxidative inactivation by reactive oxygen species (7–10). Here, we focus on the role of cholesterol in surfactant. Karagiorga et al. (11) recently reported an increase of cholesterol in surfactant from ARDS patients over control (8.5 ± 5% w/w) from 15.6 ± 2% w/w up to 43 ± 22% w/w. Cholesterol in surfactant is also increased to 20% w/w in animal models of lung injury (12). For such elevated levels of cholesterol, the lowest surface tension observed by us in vitro is 16 mN/m (13). At a surface tension of 16 mN/m, the alveoli recede from a spherical shape into shallow cavities in the terminal airways and the gas exchange area is reduced to less than one-half of its normal value (3). It was therefore concluded that an elevated level of cholesterol abolishes surfactant function.

In this study, we show by atomic force microscopy (AFM) and Kelvin probe force microscopy (KPFM) that failure of surfactant function in the presence of 20% w/w cholesterol coincides with a distinct change in the molecular architecture of the interfacial film. KPFM is an imaging mode of AFM and produces a map of the local electrical surface potential in addition to a topographical AFM image. For films of amphiphilic molecules, the electrical surface potential is a footprint of the molecular species and/or their molecular order under the tip (14–17) and arises from the alignment of molecular dipoles μ, upon packing of the film (18). More specifically, the surface potential is a function of the component of μ normal to the interface, the dielectric constant ε of the environment

Submitted February 9, 2007, and accepted for publication March 27, 2007.

Address reprint requests to M. W. Amrein, Tel.: 403-210-8177; E-mail: mamrein@ucalgary.ca.

Editor: Lukas K. Tamm.

0006-3495/07/07/674/10 $2.00

doi: 10.1529/biophysj.107.106310

of the dipoles, and the packing density of molecules (dipoles) or surface area *A* occupied by each molecule. For phospholipids, contributions have been ascribed to various regions of the molecules, each in its own dielectric environment—the headgroup region, the aliphatic tail, and the terminal methyl group (18). For example, films of dipalmitoylphosphatidylcholine, the most abundant of the surfactant components, has been reported to give rise to a surface potential of ~500 mV, at the surface tensions used in this study (26 mN/m) (19). In a film composed of many components like pulmonary surfactant, the local differences in electrical surface potential reflect the differences in local sample composition, but also packing and ordering of the molecules in an area (20).

Films for this study were formed from bovine lipid extract surfactant (BLES). BLES is a clinically used replacement surfactant. BLES differs from natural surfactant in the lack of the hydrophilic surfactant-associated proteins SP-A and SP-D as well as cholesterol. It consists of ~80% by weight of phosphatidylcholines with dipalmitoylphosphatidylcholine (DPPC) and 1-palmitoyl-2-oleoyl-phosphatidylcholine being the major molecular species and dipalmitoylphosphatidylglycerol and 1-palmitoyl-2-oleoyl-phosphatidylglycerol being present at significant levels. It also contains phosphatidylethanolamine, phosphatidylinositol, sphingomyelin, trace amounts of lyso-phosphatidic acids, and vitamin E as well as the small hydrophobic surfactant-associated proteins SP-B and SP-C (21). Cholesterol, which is removed from BLES, is the major neutral lipid in mammalian surfactant at 5–10% w/w. In the current study, films were prepared from unaltered BLES, from BLES with 5% w/w cholesterol added (reflecting normal surfactant), and BLES with 20% w/w cholesterol added (reflecting surfactant in ARDS).

MATERIALS AND METHODS

Preparation of the surfactants

BLES in nonbuffered normal saline (pH 5–6) with a phospholipid concentration of 27 mg/ml was a gift by the manufacturer (BLES Biochemical, London, Ontario). Cholesterol was purchased from Sigma Chemicals (St. Louis, MO). A solution of 1:1:1 ratio of methanol, chloroform, and BLES by volume was first vortexed and then centrifuged at 100 *g* for 5 min. The methanol/water phase was discarded and the BLES in chloroform was retained and none, 5% w/w, or 20% w/w of cholesterol, with respect to phospholipids, was added. Each solution was then dried under N_2 and resuspended with buffer (140 mM NaCl, 10 mM HEPES, and 2.5 mM CaCl2; pH 6.9) to obtain an aqueous suspension of BLES and cholesterol at a concentration of 27 mg/ml phospholipids.

Film deposition

For the microscopy, the films were deposited onto freshly cleaved mica (ruby, ASTMV-2 quality, Asheville-Schoonmaker Mica, Newport News, VA) by the Langmuir-Blodgett technique. Surfactant suspensions were spread at the air-buffer interface (750 cm^2) of a Langmuir trough (Nima Technology, Coventry, England) at room temperature. The film area was reduced or expanded at a rate of 100 cm^2/min, the surface tension continuously monitored, and area-surface tension isotherm recorded (Fig. 1). For results shown in Figs. 2–5 and 6, films were contracted or expanded before deposition by defined amounts as described in the following section. For deposition, a mica support was first lowered across the interface at a speed of 45 mm/min and then retracted at 25 mm/min. A film was deposited upon the upstroke while the surface tension was kept constant.

For the films shown in Fig. 4 or discussed in the Results, a first sample of each film was deposited onto mica upon the film contraction at a surface tension of $\gamma = 34$ mN/m (denoted by *1* in Fig. 1, denoted *expanded* in Fig. 4). A second sample was collected at $\gamma = 26$ mN/m in a similar way (denoted by *2* in Fig. 1, denoted *contracted* in Fig. 4). A third sample was collected at $\gamma = 34$ mN/m (denoted by *3* in Fig. 1, denoted *re-expanded* in Fig. 4) after the film area had been reexpanded. The collection points were chosen such that upon area reduction, the first sample was taken before the onset of a shoulder in area-surface tension isotherm, the second sample at the end of the shoulder, and the third sample after a partial reexpansion of the film (Fig. 1). For the results shown in Figs. 5 and 6, films were obtained similar to collection point 2 (after ~50% area reduction from the onset of the shoulder in surface tension isotherm).

Microscopy

AFM topographical images were collected in air with a NanoWizard AFM (JPK Instruments, Berlin, Germany) using noncontact mode silicon cantilevers NCH-20 from NanoWorld with typical spring constants of 21–78 N/m, and resonance frequencies of 260–460 kHz.

Surface potential maps and corresponding topographical images were acquired on two different instruments employing two different methods of measuring the electrical surface potential. Both methods revealed similar potentials for corresponding film areas. The data displayed in Fig. 5, *A* and *B*, and Fig. 6 *A* were collected in air with a NanoWizard AFM. The images were acquired by tracing the sample areas line by line. On trace, the sample the topography was measured in intermittent contact mode. On the return pass (retrace), the height information was used to maintain the cantilever at a

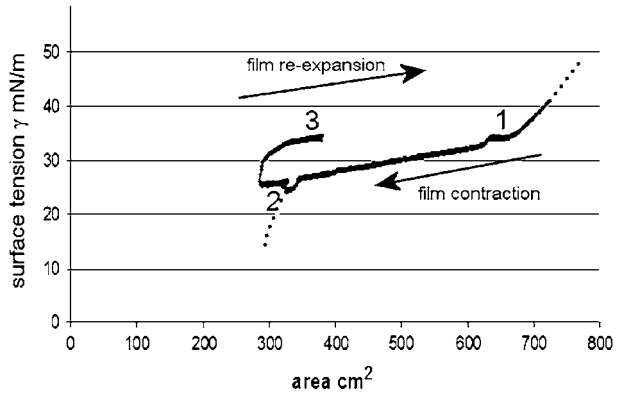

FIGURE 1 Area-surface tension isotherm of BLES upon sample collection. The solid black line denotes the isotherm. Upon contraction of the film, the surface tension first dropped steeply before flattening into a shoulder of the isotherm. At the inflection point, a first sample was collected (denoted by *1*). The film transfer is visible as a short horizontal stretch in the isotherm. The film area was then further reduced until the surface tension started to drop more steeply again, at which point a second sample was collected (*2*). After transfer of the second sample, the film was reexpanded and a third sample collected (*3*). Dotted lines denote the likely progression of the isotherm in the absence of sample collection. The expected progression was deduced from an isotherm of this film acquired before collection of the samples.

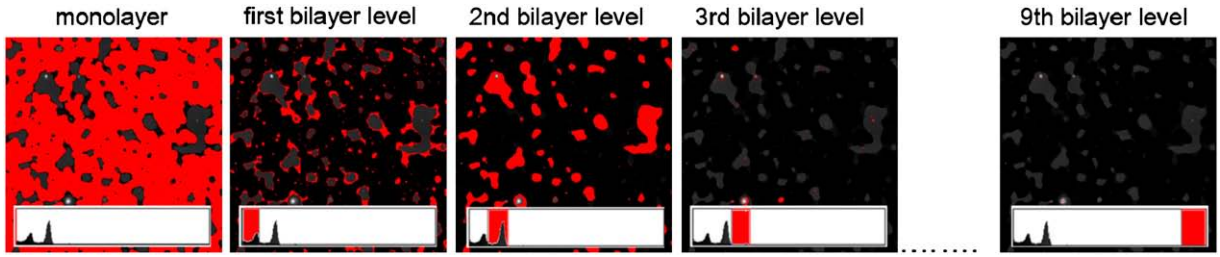

FIGURE 2 The discrete levels of lipid bilayer patches on top of each other were identified in each AFM micrograph in the histogram of the area count over topographical height using ImageJ (Wayne Rasband, National Institutes of Health, Bethesda, MD). In this example, a maximum of nine discrete levels of bilayers were identified.

constant offset height above the surface and the electrical surface potential measured as described (22). Conductive cantilevers (Type BS-ElectriTap300, BudgetSensors, Sofia, Bulgaria) were used and connected to an external circuit to control the tip potential. The high magnification image of Fig. 6 *B* was acquired, using a laboratory-built setup described in the literature (23,24). With this setup, potential and topography were measured simultaneously, using the frequency modulation technique (FM-KPFM). This method derives a surface potential by measuring the gradient of the electrostatic force rather than the force itself and is largely insensitive to the geometry of the tip.

The potential maps in this study show relative values. A value of 0 V was assigned to the most negative value in each of the maps displayed. The absolute potentials are measured by the instruments, but carry an offset due to a contact potential, brought about by the sample support to which the measured potential is referred. This is discussed in Leonenko et al. (20).

Quantitative image analysis

The total area of lipid leaflets within bilayer stacks in the AFM micrographs was computed to determine the extent by which the surfactant monolayer folded into stacks of bilayers upon the area reduction between collection points 1 and 2. For the analysis, it was assumed that the lowest topographical level in each micrograph represented a lipid monolayer. Hence, the image size equaled the monolayer area. A plateau ~5 nm above the monolayer was considered a lipid bilayer (i.e., two leaflets of lipid monolayer) on top of the monolayer; a plateau of 10 nm height was considered a monolayer with two bilayers on top of each other; etc. The total amount of lipid leaflets within bilayer stacks was then related to the area change that has occurred within the shoulder of the area-surface tension isotherm. For example, if the film area had been reduced by half between collection points 1 and 2, and the area of lipid leaflets within bilayer stacks summed up to be similar to the image size, the monolayer-bilayer conversion was considered 100%.

For each concentration of cholesterol in BLES and each of the three collection points, four micrographs from two independent experiments were analyzed.

RESULTS

Structure-function relationship of the surfactant films

The structures formed by surfactant films containing none, 5%, or 20% w/w cholesterol were related to our earlier functional study on these films (13). Films containing none or 5% reduce the surface tension close to zero mN/m and are considered functional. Films containing 20% cholesterol are unable to lower the surface tension below ~16 mN/m. A surface tension of 16 mN/m is not low enough for proper lung function.

The functional surfactants show lamellar structures scattered over the monolayer surface (Fig. 3). Each step in a stack is 5 nm high, indicative of a single lipid bilayer. The bilayer stacks form from the monolayer upon contraction. This monolayer-multilayer conversion corresponds to a shoulder in the area-surface tension isotherm (Fig. 1, see also (13)), where the surface tension changes little upon a change of ~25–50% in surface area. Before the shoulder, the films show none or only a few lamellar structures (Fig. 4, *A* and *B*, *expanded*). At the end of the shoulder, the bilayer stacks have fully established (Fig. 4, *A* and *B*, *contracted*). Our earlier functional study of these samples show that, at this point, the films have become incompressible and the surface tension drops steeply, often to <1 mN/m upon further film contraction (13). Formation of lamellar structures is reversible: the lamellar structures unfold into the monolayer (Fig. 4, *A* and *B*, *re-expanded*).

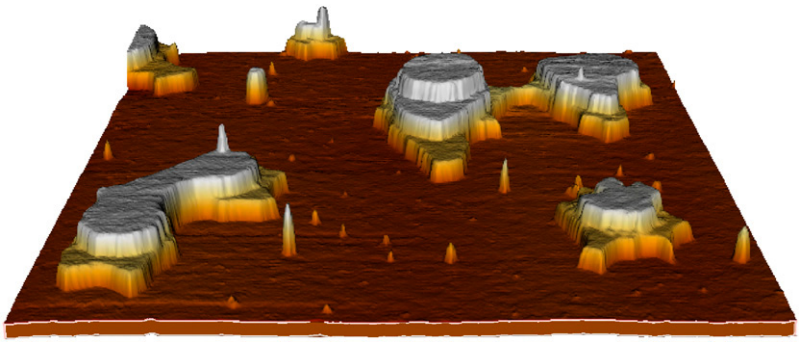

FIGURE 3 AFM micrograph in three-dimensional representation of surfactant containing 5% w/w cholesterol (5 μm × 5 μm). The film shows stacks of bilayers up to three layers high. Each layer is five nanometers high.

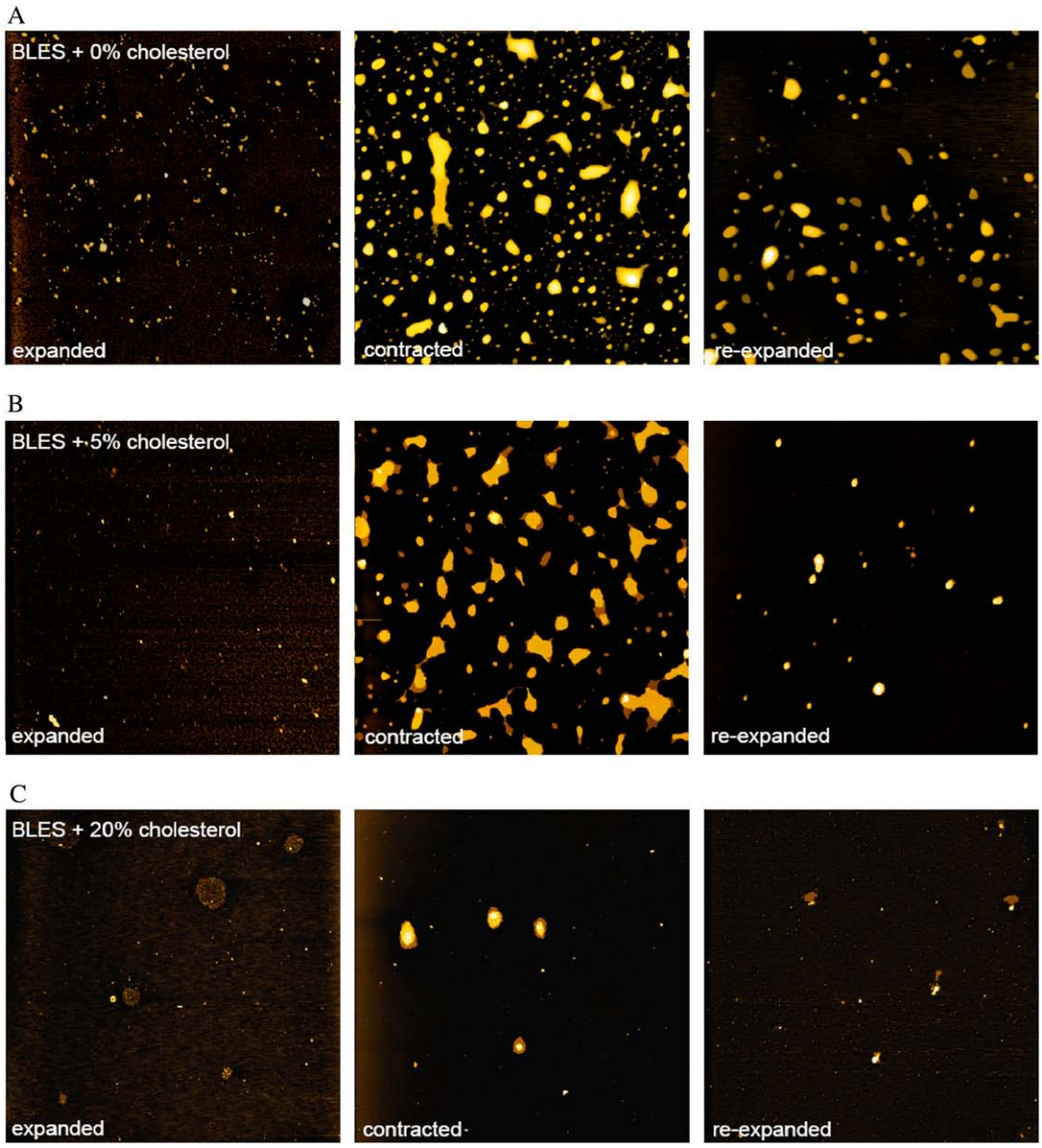

FIGURE 4 AFM topographies (20 μm $\times$ 20 μm) of BLES containing no cholesterol (*A*), 5% w/w cholesterol (*B*), and 20% w/w cholesterol (*C*). The films denoted ''expanded'' have been collected from the Langmuir trough after the film was spread and allowed to contract up to the onset of a shoulder in the area-surface tension isotherm ($\gamma = 34$ mN/m, see Fig. 1). Then, the film area was further reduced and another sample collected (denoted *contracted*; ($\gamma =$ 26 mN/m)). The images in the right column have been acquired from films after a partial reexpansion ($\gamma = 34$ mN/m). Films containing no or 5% cholesterol formed stacks of lipid bilayer patches, attached to the monolayer. The bilayer patches reintegrated in the monolayer when the film was reexpanded. Note that the reexpanded films of panels *A* and *B* still show some bilayer stacks because the area was only partially reexpanded. Films with 20% cholesterol formed almost no lipid bilayer stacks and continuously collapsed during contraction (*C*).

The amount of area reduction required to reach a surface tension of 26 mN/m varied between ~40% and 50% of the area after the first sample was collected. The amount of reexpansion required to reach a surface tension of 34 mN/m was also different for each film and varied from ~50–30% of the area change that had previously occurred between collection points 1 and 2. The amount of reexpansion was less than the previous contraction because of a hysteresis between the contraction and expansion trace (Fig. 1; i.e., the surface tension rose faster on the expansion as it had previously dropped on contraction). For the film shown in Fig. 4 *A*, the area between sample collections has been reduced from the expanded state (100%) to ~50% and then was reexpanded to ~75% for collection of the film denoted ''re-expanded.'' The variability between isotherms of similar samples is discussed in Gunasekara et al. (13).

For films containing 20% cholesterol, the AFM micrographs reveal almost no lamellar structures (Fig. 4 *C*). Lack

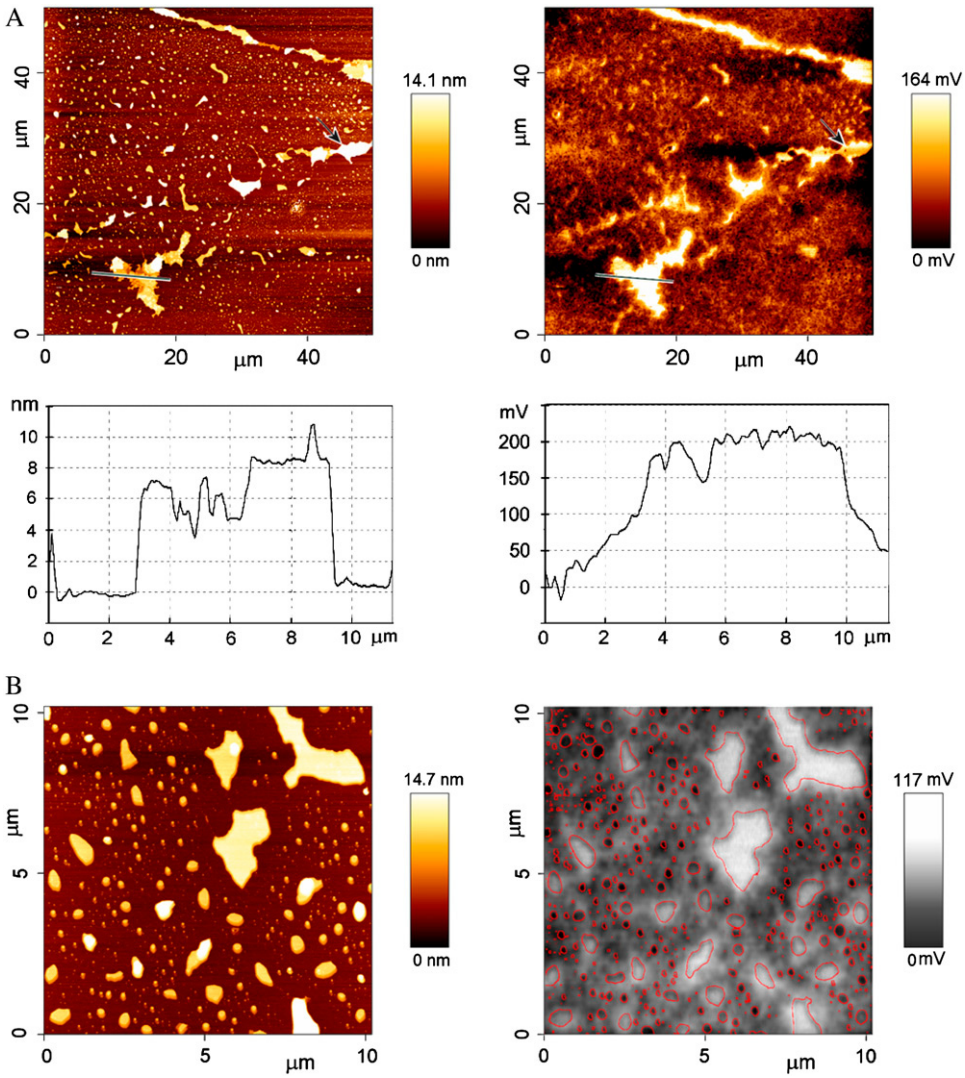

FIGURE 5 (*A*) Overview of a film of BLES that contains no cholesterol. The topographical image (*left*, and *cross section below*) shows a pattern of monolayer and scattered multilayer regions. In the potential map (*right*, and *cross section below*) large stacks of bilayer patches are at a potential of up to 200 mV above the monolayer. The arrows in the topographical image and in the potential map point to a region, where the topographical height does not change but the potential shows two distinct levels. (*B*) BLES film at higher magnification. The outer perimeters of the bilayer stacks from the topological image (*left*) are overlaid in red in the potential map (*right*). The larger of the bilayer stacks are at positive potential with respect to the monolayer. Small stacks are up to ~100 mV lower in the electrical potential than average.

of lamellar structures is consistent with a continuous, irreversible collapse of monolayer matter into the aqueous phase upon contraction of the film. The area reduction required to reach 26 mN/m was only ~20% for the films containing 20% cholesterol. We therefore also collected films after ~50% area reduction, at which point the surface tension had dropped to ~20 mN/m. These films too were devoid of bilayer stacks (not shown).

Quantitative analysis of the micrographs from expanded and contracted films allowed for an estimate of the proportion of lipids that underwent a monolayer-bilayer conversion over the lipids that were lost to the aqueous phase upon film contraction (Fig. 2; and see Materials and Methods). The estimate was based on the analysis of four micrographs such as shown in Fig. 4 for each condition. According to this analysis, for surfactant containing no cholesterol, 100% of the lipids in the monolayer displaced from the interface were recovered in bilayer stacks. Individual micrographs ranged from 100 to 103% recovery. For films containing 5% w/w cholesterol, ~12% of the squeezed lipids were lost to the subphase and, hence, ~88% converted into stacks of bilayers after the film area had been reduced by half. Individual micrographs ranged from 5 to 18% loss. For films containing 20% w/w cholesterol, >90% of the lipids were lost to the aqueous phase upon contraction.

The structure of the bilayer stacks as revealed by Kelvin probe force microscopy

Fig. 5 shows the topography (*left*) and local electrical surface potential (*right*) of films containing no cholesterol. Both the topographical map and the electrical surface potential map (*right*) are highly structured for these films, and the dynamic range of the electrical signal is 300–400 mV. Large stacks of bilayer patches are at a potential of up to 200 mV above the monolayer. Upon close inspection of Fig. 5 *A*, including the cross-sections below the respective images, the potential is not strictly correlated with topographical height (i.e., film

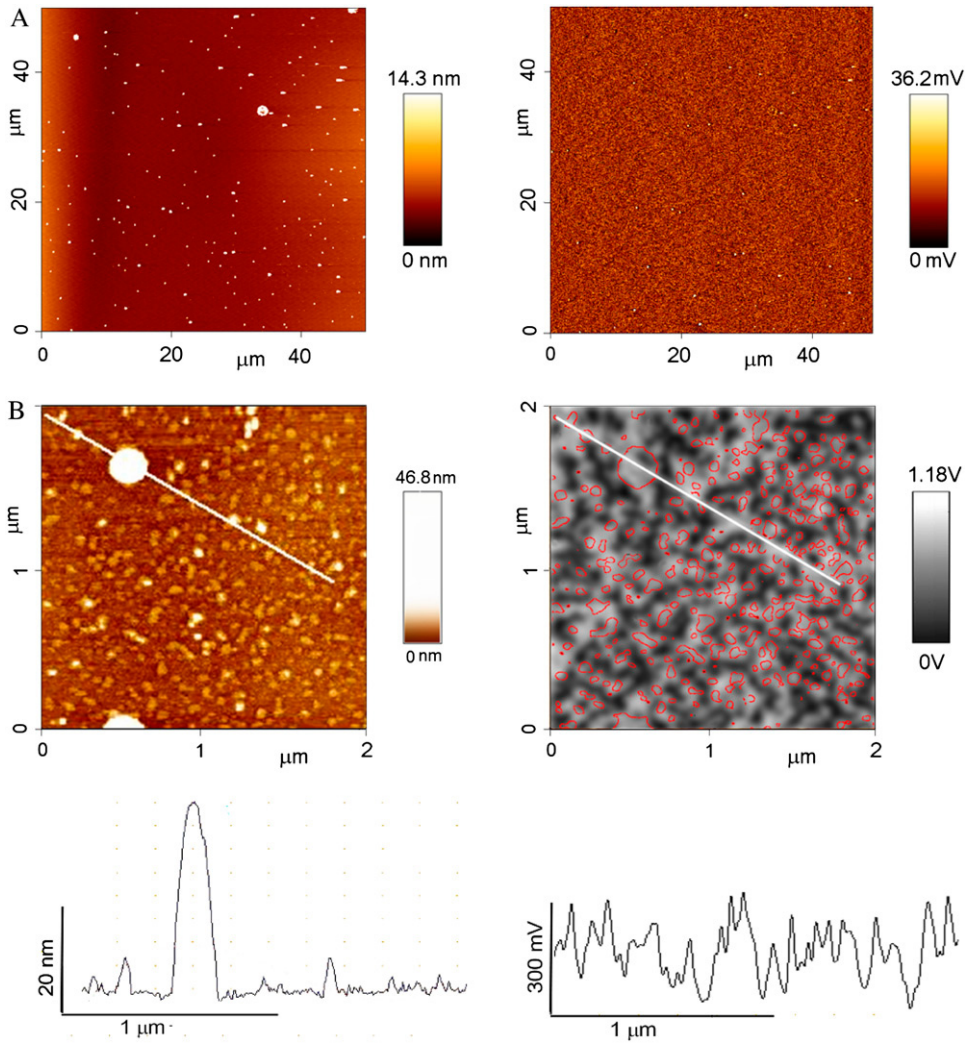

FIGURE 6 (*A*) Overview of a film of BLES that contains 20% cholesterol by weight. Protrusions in the topographical image (*left*) are not different in the potential map (*right*). (*B*) A high-resolution map of the topography (*left*) and potential (*right*) of the film containing 20% cholesterol. The perimeter of the small topographical features were computed from the topographical image and overlaid in red on the potential map. The monolayer is strongly electrically structured with a dynamic range of up to 300 mV. The length scale of the electrical domains is ~100 nm. The perimeters shown in the overlay are enclosing an area of larger topographical height (i.e., larger film thickness). In the potential map, these areas coincide with the regions at a more positive surface potential.

thickness). Sometimes the potential even drops to a lower level within an area of constant topographical height (*arrows* in Fig. 5 *A*).

Fig. 5 *B* shows the film at higher magnification. To allow for easy correlation between topology and potential, the outer perimeters of the bilayer stacks were computed from the AFM topographical image (Fig. 5 *B*, *left*) and overlaid in red in the potential map (Fig. 5 *B*, *right*). Interestingly, only the larger, irregularly shaped bilayer-stacks are always at a more positive voltage with respect to the average potential. Smaller stacks have an almost spherical perimeter. The stacks between 200 and 400 nm in diameter are either at a more negative or more positive potential. Smaller stacks are up to ~100 mV below average potential.

The most striking feature in the surface potential maps is the either positive or negative surface potential of the stacks of lipid bilayers with respect to the monolayer areas. The large contributions of the stacks to the surface potential may not likely be ascribed to lipids. The lipids of the two leaflets of a bilayer are of opposite orientation with respect to the sample plane such that the contribution to the surface potential cancels out. Rather, the surface potential difference to the monolayer observed for most of the stacks may find its explanation by the presence of the small hydrophobic surfactant-associated protein SP-C. SP-C consists mostly of an α-helical segment that spans lipid bilayers (25,26). Alpha-helices exhibit a strong molecular dipole moment along the helix axis, which, in the case of SP-C, may be accentuated by positive charges near its N-terminus. SP-C promotes the formation of lipid bilayer patches and resides in these multilamellar regions of the surfactant films (27). Note that the absolute contribution of the SP-C to the surface potential of the lipid stacks will be reduced by the screening of the helical dipole in the lipid environment (28).

If SP-C is indeed the cause for the observed surface potential of the bilayer stacks, it is not randomly oriented. A positive surface potential such as observed for the large stacks is caused when a majority or all SP-C molecules in an area span the lipid bilayers in a stack with the N-terminus pointing toward the air. If SP-C is arranged with its C-terminal end toward the air, the bilayer stacks will be at a more negative potential than the monolayer such as observed with the small

stacks. The extended irregularly shaped bilayer stacks shown in Fig. 5 *A* may have arisen from multiple folding events and/or the fusion of smaller stacks. This would explain why, in a region of constant topographical height, the electrical surface potential sometimes changes in stepwise fashion, as outlined by the arrows in Fig. 5 *A*.

SP-B is also present in BLES and also promotes the formation of lamellar structures (29,30). SP-B is likely composed of four to five amphipathic helices (i.e., helices with a highly hydrophobic face on the one side and a hydrophilic face on the opposite side of the helix-axis; for reviews, see (31,32). It is proposed that the helices are aligned partially immersed in the lipid layer with the axis parallel to the interface (33) and act as a cross-linker between monolayer and bilayer patches. Since the helix-dipoles in this case are parallel to the interface, they should not contribute to the surface potential. However, being immersed only in one of the two leaflets of a bilayer might introduce sufficient asymmetry for a bilayer to show a net surface potential.

The elevated surface potential of the large bilayer stacks immediately drops by ~100 mV outside the perimeter of the large bilayer stacks (*cross sections*, Fig. 5 *A*). Further reduction of the potential by ~50–100 mV occurs gradually over a distance of ~1 μm, indicating that the molecular composition and order of the monolayer gradually changes toward the stacks. We have shown earlier that SP-C becomes gradually inserted from the monolayer into the bilayer stacks upon area reduction (27,34,35). Hence, SP-C may still be present also in the monolayer close to the stacks in Fig. 5 and induce an elevated surface potential. SP-B appears to also become gradually integrated in bilayer stacks upon film contraction (30) and could have a similar effect. The monolayer close to the stacks may also have a different lipid composition.

For the films containing 20% cholesterol, (Fig. 6), the occasional protrusions are not at an elevated electrical potential with respect to the monolayer. The absence of a contrast in the Kelvin signal in this case may either reflect a disordered molecular arrangement, where molecular dipoles cancel out, or bilayers devoid of protein. This indicates that cholesterol inhibits the ordered monolayer-bilayer conversion promoted by SP-B and/or SP-C. Furthermore, unlike in the absence of cholesterol, the surface potential is also not altered in the monolayer in proximity to the (rare) protrusions. Hence, given the role ascribed to SP-B and/or SP-C in shaping the surface potential maps of films devoid of cholesterol, these proteins may have been lost early on upon contraction for the films containing 20% cholesterol.

At high resolution of the films containing 20% cholesterol (Fig. 6 *B*), electrical domains in the monolayer region become visible. The domains are ~100 nm across and, hence, too small to be resolved in the low magnification map shown in Fig. 6 *A*. The dynamic range of the potential of the domains is ~300 mV. On close inspection, regions of slightly greater film thickness are found to coincide with regions at a more positive surface potential. Electrical domains of this size are not present in films containing no cholesterol. Hence, cholesterol causes also the lipids in the monolayer to become differently arranged. In fluorescence light microscopy, surfactant containing no cholesterol segregates into domains. Condensed domains, typically several micrometers across, are surrounded by the more fluid components in the film (e.g., (35–39)). Surfactants containing cholesterol, on the other hand, appear homogenous by light microscopy (38,39). Our study now shows that these films still form domains, but they are too small to be resolved in a light microscope. Areas of higher potential are always found in topographically elevated areas. Cholesterol promotes a more positive surface potential in phospholipid films (40) and may therefore reside in the elevated (thicker) film areas.

DISCUSSION

Our experimental findings indicate that the function of pulmonary surfactant films depends on the presence of bilayer stacks. The stacks are reversibly formed from the monolayer during film contraction and reinsert into the monolayer upon reexpansion. An elevated level of cholesterol inhibits the monolayer-bilayer conversion and results in dysfunctional films. In this Discussion, we will attribute the unique mechanical properties observed with the functional surfactant partially to sorting of the surfactant components between the monolayer and adjacent bilayer patches and partially to mechanical reinforcement of the film by the bilayer stacks.

Sorting

The minimum surface tension achievable by unsaturated phospholipids is ~20–30 mN/m. DPPC films, on the other hand, can attain near-zero surface tension. During monolayer-bilayer conversion, unsaturated lipids may be transferred from the monolayer to the adjacent bilayer patches. The monolayer may thus become enriched in DPPC, which allows for low surface tension. If the monolayer-bilayer conversion is inhibited by an excess amount of cholesterol, the unsaturated lipids remain in the monolayer and a low surface tension cannot be achieved. Instead, the film continuously collapses upon contraction.

The notion of a monolayer-bilayer conversion that also involves sorting of lipids is supported by the unique properties of SP-C in conjunction with our experimental finding of a defined orientation and polarity of SP-C within the stacks. Fig. 7 depicts how the orientation of SP-C may become defined by the two palmitoyl groups close to the N-terminus during film contraction. In this model, the palmitoyl groups remain anchored in the monolayer while the helix moves together with the lipids into a newly formed bilayer toward the aqueous phase. An inverted bilayer patch, formed toward the air, causes the opposite orientation of the SP-C molecule. The palmitoyl groups are likely to remain anchored to the monolayer because of their strong affinity to domains of condensed, saturated lipids (41). Condensed DPPC domains

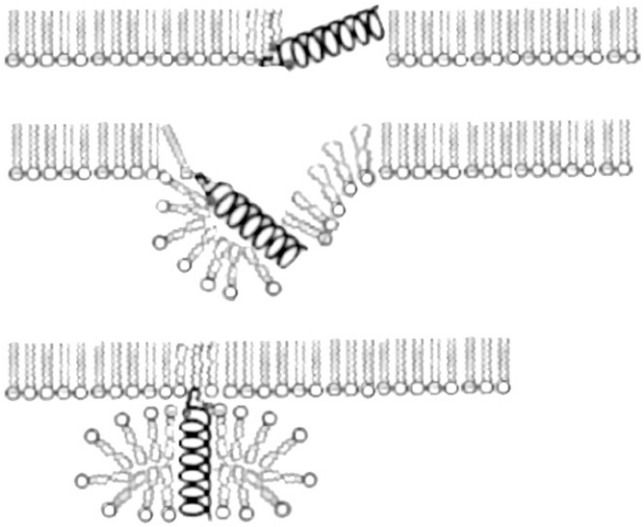

FIGURE 7 Mechanism explaining a positive surface potential on the large bilayer stacks. The helical span of SP-C is oriented in lipid monolayers with ~70° to the normal of the interface (51). Upon film contraction, a first bilayer adjacent to the monolayer is formed toward the aqueous subphase. SP-C rotates to span the newly formed bilayer and remains anchored to the monolayer by its two palmitoyl groups near its N-terminal end. SP-C is known to span lipid bilayers (52). As a result, all SP-C molecules face with the N-terminus toward the air, resulting in a positive surface potential. A related mechanism (not shown) may occur for the small bilayer stacks that were found to be at negative electrical surface potential. This time, the bilayer stacks may form toward the air. With the highly hydrophilic N-terminus remaining immersed in the water phase, SP-C may now point with its C-terminus toward the air.

are common for both model and natural surfactant films (e.g., (42)). In accordance with this proposed role of the palmitoyl anchor, we found earlier in a model surfactant containing SP-C that bilayer stacks were always associated with condensed regions of a phase-separated monolayer and were excluded from the more fluid regions of the film (43). While the palmitoyl-groups of the SP-C are likely associated with DPPC in the monolayer at the air-water interface, the helical part of the SP-C is known to span lipid bilayers in a fluid state and is excluded from bilayers in the condensed gel phase (25). This suggests that SP-C promotes formation of bilayer patches of unsaturated lipids.

While pulmonary surfactant function may depend on the monolayer-bilayer conversion to remove unsaturated lipids from the monolayer, the monolayer-bilayer conversion does not necessarily depend on the presence of unsaturated lipids. The conversion occurs even in the presence of only saturated lipids (DPPC, dipalmitoyl phosphatidyl glycerol) and SP-C (35) and can be inhibited by an excess amount of cholesterol as well (44).

Reinforcement

Sorting and a pure or enriched DPPC monolayer alone cannot fully account for the mechanical stability of a functional surfactant film by itself. Pure DPPC monolayers, while capable of sustaining a near-zero surface tension, collapse irreversibly when mechanically disturbed or overcompressed after reaching close-to-zero surface tension (45). To understand why the monolayer-bilayer conversion is required for stability at close-to-zero surface tension, the bilayer stacks may be ascribed a mechanical role, similar to the role of reinforcing elements in preventing a thin plate from collapsing under lateral compression (46). In this analogy, the surface tension is equivalent to an external lateral pressure compressing a plate and the molecular film is the continuum plate. The film will buckle above a critical compression. Buckling has been described as a mode of failure for pulmonary surfactant (47). Qualitatively, having lipid bilayer patches on the surface breaks the large areas into smaller patches. According to elastic theory, the compression above which collapse occurs, increases strongly with a decrease in size of the elements for a given cross section (or film thickness) (46). For the bilayer stacks to be mechanically reinforcing, they must be cross-linked to the monolayer. Otherwise, they will separate from, or glide over, the monolayer upon area reduction and have no mechanical effect. In the mechanism for the formation of stacks proposed above (Fig. 7), SP-C acts as the cross-linker. We earlier found direct evidence for cross-linkage by SP-C by mechanically manipulating bilayer stacks in a surfactant model containing SP-C (43). SP-B is also acting as a cross-linker, and on its own has led to the formation of bilayer stacks in a model surfactant film of exceptional stability (48). In agreement with this proposed function of SP-C and SP-B, artificial or animal extract surfactants depend on the presence of either one or both hydrophobic proteins to lower the surface tension to a physiological low level.

Cholesterol inhibits the monolayer-bilayer conversion. It thus affects both purification of the monolayer from unsaturated lipid species and reinforcement of the film by the bilayer stacks. Cholesterol does not appear to cause monolayer instability independent of these mechanisms. Our earlier study of surfactant function (13) revealed that BLES films can attain a very low surface tension even in the presence of 20% cholesterol, if the relative amount of DPPC is also increased by the same proportion as the cholesterol. We now found that, under these conditions, the monolayer-bilayer conversion is still mostly inhibited (not shown). Hence, these films may already contain a sufficient proportion of DPPC to allow for a low surface tension and may therefore not depend on the monolayer-bilayer conversion for sorting. However, the functional study (13) also showed that, while attaining a surface tension close to zero, the films were otherwise inferior to a fully functional film. The films required an unphysiologically large amount of area reduction to lower the surface tension close to zero. They also became dysfunctional after repeated expansion and compression (13). Hence, similar to pure DPPC films, these films lacked stability at near-zero surface tension. We ascribe lack of stability to the absence of the reinforcing bilayer stacks.

CONCLUSIONS

An elevated level of cholesterol inhibits the reversible monolayer-bilayer conversion in pulmonary surfactant and thus leads to failure of surfactant function. Cholesterol should therefore become a target for treatment of surfactant impairment in ARDS. To find ways to reverse the effect of excess cholesterol, future studies will have to address the mechanism by which cholesterol inhibits the monolayer-bilayer conversion. An effective treatment, in addition to countering the effect of cholesterol, may also have to target other mechanisms of surfactant inhibition, including oxidation of surfactant through the reactive oxygen species present in the injured lung (7–10,49) and interference with serum proteins that interact with surfactant (e.g., (50)).

We are grateful to BLES Biochemicals, London, Ontario for generously providing BLES. We thank Dr. Elmar Prenner for his valuable discussions and for making the Langmuir surface balance accessible to us. We thank Drs. Richard Leigh, Samuel Schurch, Ayo Jeje, and Peter Tieleman for corrections and valuable discussions.

This research has been supported by the Canadian Institute of Health Research, Alberta Children's Hospital Foundation (to M.A.), Alberta Lung Association (to M.A.), and the Canada Foundation for Innovation.

REFERENCES

1. von Neergard, K. 1929. New views on a subject of the mechanics of breathing: the retractive force of the lung in dependence of the surface tension in the alveoli. *Z. Ges. Exp. Med.* 66:373–381.
2. Schurch, S. 1982. Surface tension at low lung volumes: dependence on time and alveolar size. *Respir. Physiol.* 48:339–355.
3. Bachofen, H., and S. Schurch. 2001. Alveolar surface forces and lung architecture. *Comp. Biochem. Physiol.* 129:183–193.
4. Lewis, J. E., and R. Veldhuizen. 2003. The role of exogenous surfactant in the treatment of acute lung injury. *Annu. Rev. Physiol.* 65:613–642.
5. Taeusch, H. W., and K. M. W. Keough. 2001. Inactivation of pulmonary surfactant and the treatment of acute lung injury. *Pediatr. Pathol. Mol. Med.* 20:519–536.
6. Taeusch, H. W., J. B. de la Serna, J. Perez-Gil, C. Alonso, and J. A. Zasadzinski. 2005. Inactivation of pulmonary surfactant due to serum-inhibited adsorption and reversal by hydrophilic polymers: experimental. *Biophys. J.* 89:1769–1779.
7. Rodriguez-Capote, K., D. Manzanares, T. Haines, and F. Possmayer. 2006. Reactive oxygen species inactivation of surfactant involves structural and functional alterations to surfactant proteins SP-B and SP-C. *Biophys. J.* 90:2808–2821.
8. Andersson, S., A. Kheiter, and T. A. Merritt. 1999. Oxidative inactivation of surfactants. *Lung.* 177:179–189.
9. Mark, L., and E. P. Ingenito. 1999. Surfactant function and composition after free radical exposure generated by transition metals. *Am. J. Physiol. Lung Cell. Mol. Physiol.* 276:L491.
10. Gilliard, N., G. P. Heldt, J. Loredo, H. Gasser, H. Redl, T. A. Merritt, and R. G. Spragg. 1994. Exposure of the hydrophobic components of porcine lung surfactant to oxidant stress alters surface-tension properties. *J. Clin. Invest.* 93:2608–2615.
11. Karagiorga, G., G. Nakos, E. Galiatsou, and M. E. Lekka. 2006. Biochemical parameters of bronchoalveolar lavage fluid in fat embolism. *Intensive Care Med.* 32:116–123.
12. Panda, A., K. Nag, R. Harbottle, K. V. Rodriguez-Capote, A. Ruud, W. N. Petersen, and O. F. Possmayer. 2004. Effect of acute lung injury on structure and function of pulmonary surfactant films. *Am. J. Respir. Cell Mol. Biol.* 30:641–650.
13. Gunasekara, L., S. Schurch, W. M. Schoel, K. Nag, Z. Leonenko, M. Haufs, and M. Amrein. 2005. Pulmonary surfactant function is abolished by an elevated proportion of cholesterol. *Biochim. Biophys. Acta-Mol. Cell Biol. Lipids.* 1737:27–35.
14. Chi, L. F., S. Jacobi, and H. Fuchs. 1996. Chemical identification of differing amphiphiles in mixed Langmuir-Blodgett films by scanning surface potential microscopy. *Thin Solid Films.* 284–285:403–407.
15. Jacobi, S., L. F. Chi, and H. Fuchs. 1996. Combined scanning force, lateral force, and scanning surface potential microscopy on phase-separated Langmuir-Blodgett films. *J. Vac. Sci. Technol. B.* 14:1503–1508.
16. Lu, J., E. Delamarche, L. Eng, R. Bennewitz, E. Meyer, and H. J. Guntherodt. 1999. Kelvin probe force microscopy on surfaces: investigation of the surface potential of self-assembled monolayers on gold. *Langmuir.* 15:8184–8188.
17. Knapp, H. F., P. Mesquida, and A. Stemmer. 2002. Imaging the surface potential of active purple membrane. *Surf. Interface Anal.* 33:108–112.
18. Dynarowicz-Latka, P., A. Dhanabalan, and O. N. Oliveira, Jr. 2001. Modern physicochemical research on Langmuir monolayers. *Adv. Colloid Interf. Sci.* 91:221–293.
19. Brockman, H. 1994. Dipole potential of lipid membranes. *Chem. Phys. Lipids.* 73:57–79.
20. Leonenko, Z., M. Rodenstein, J. Dohner, L. M. Eng, and M. Amrein. 2006. Electrical surface potential of pulmonary surfactant. *Langmuir.* 22:10135–10139.
21. Yu, S. H., and F. Possmayer. 2003. Lipid compositional analysis of pulmonary surfactant monolayers and monolayer-associated reservoirs. *J. Lipid Res.* 44:621–629.
22. Nonnenmacher, M., M. P. O'Boyle, and H. K. Wickramasinghe. 1991. Kelvin probe force microscopy. *Appl. Phys. Lett.* 58:2921–2923.
23. Zerweck, U., C. Loppacher, T. Otto, S. Grafstrom, and L. M. Eng. 2005. Accuracy and resolution limits of Kelvin probe force microscopy. *Phys. Rev. B.* 71:125424–125433.
24. Loppacher, C., U. Zerweck, S. Teich, E. Beyreuther, T. Otto, S. Grafstrom, and L. M. Eng. 2005. FM demodulated Kelvin probe force microscopy for surface photovoltage tracking. *Nanotechnology.* 16:S1–S6.
25. Johansson, J., T. Szyperski, T. Curstedt, and K. Wüthrich. 1994. The NMR structure of the pulmonary surfactant-associated polypeptide SP-C in an apolar solvent contains a valyl-rich α-helix. *Biochemistry.* 33:6015–6023.
26. Johansson, J., T. Szyperski, and K. Wüthrich. 1995. Pulmonary surfactant-associated polypeptide SP-C in lipid micelles: CD studies of intact SP-C and NMR secondary structure determination of dipalmitoyl-SP-C (1–17). *FEBS Lett.* 362:261–265.
27. Kramer, A., A. Wintergalen, M. Sieber, H. J. Galla, M. Amrein, and R. Guckenberger. 2000. Distribution of the surfactant-associated protein C within a lung surfactant model film investigated by near-field optical microscopy. *Biophys. J.* 78:458–465.
28. Sengupta, D., R. N. Behera, J. C. Smith, and G. M. Ullmann. 2005. The alpha helix dipole: screened out? *Structure.* 13:849–855.
29. Lipp, M. M., K. Y. Lee, J. A. Zasadzinski, and A. J. Waring. 1996. Phase and morphology changes in lipid monolayers induced by SP-B protein and its amino-terminal peptide. *Science.* 273:1196–1199.
30. Krol, S., M. Ross, M. Sieber, S. Kunneke, H. J. Galla, and A. Janshoff. 2000. Formation of three-dimensional protein-lipid aggregates in monolayer films induced by surfactant protein B. *Biophys. J.* 79:904–918.
31. Hawgood, S., M. Derrick, and F. Poulain. 1998. Structure and properties of surfactant protein B. *Biochim. Biophys. Acta.* 1408:150–160.
32. Serrano, A. G., and J. Perez-Gil. 2006. Protein-lipid interactions and surface activity in the pulmonary surfactant system. *Chem. Phys. Lipids.* 141:105–118.
33. Andersson, M., T. Curstedt, H. Jornvall, and J. Johansson. 1995. An amphipathic helical motif common to tumorolytic polypeptide NK-lysin and pulmonary surfactant polypeptide SP-B. *FEBS Lett.* 362:328–332.

34. Amrein, M., A. von Nahmen, and M. Sieber. 1997. A scanning force- and fluorescence light microscopy study of the structure and function of a model pulmonary surfactant. *Eur. Biophys. J.* 26:349–357.

35. von Nahmen, A., M. Schenk, M. Sieber, and M. Amrein. 1997. The Structure of a model pulmonary surfactant as revealed by scanning force microscopy. *Biophys. J.* 72:463–469.

36. Post, A., A. V. Nahmen, M. Schmitt, J. Ruths, H. Riegler, M. Sieber, and H. J. Galla. 1995. Pulmonary surfactant protein C containing lipid films at the air-water interface as a model for the surface of lung alveoli. *Mol. Membr. Biol.* 12:93–99.

37. von Nahmen, A., A. Post, H. J. Galla, and M. Sieber. 1997. The phase behavior of lipid monolayers containing pulmonary surfactant protein C studied by fluorescence light microscopy. *Eur. Biophys. J.* 26:359–369.

38. Panda, A. K., A. Hune, K. Nag, R. R. Harbottle, and N. O. Petersen. 2003. Structural alterations of phospholipid film domain morphology induced by cholesterol. *Indian J. Biochem. Biophys.* 40:114–121.

39. Discher, B. M., K. M. Maloney, D. W. Grainger, and S. B. Hall. 2002. Effect of neutral lipids on coexisting phases in monolayers of pulmonary surfactant. *Biophys. Chem.* 101–102:333–345.

40. Mozaffary, H. 1994. Cholesterol-phospholipid interaction: a monolayer study. *Thin Solid Films.* 244:874–877.

41. Simons, K., and D. Toomre. 2000. Lipid rafts and signal transduction. *Nat. Rev. Mol. Cell Biol.* 1:31–39.

42. Nag, K., J. Perez-Gil, M. L. Ruano, L. A. Worthman, J. Stewart, C. Casals, and K. M. Keough. 1998. Phase transitions in films of lung surfactant at the air-water interface. *Biophys. J.* 74:2983–2995.

43. Amrein, M., D. Knebel, and M. Haufs. 2005. Structure and function of the molecular film of pulmonary surfactant at the air-alveolar interface: the role of SP-C. *In* Molecular Mechanisms in Lung Surfactant (Dys)Function. K. Nag, editor. Marcel Dekker, New York.

44. Malcharek, S., A. Hinz, L. Hilterhaus, and H. J. Galla. 2005. Multilayer structures in lipid monolayer films containing surfactant protein C: effects of cholesterol and POPE. *Biophys. J.* 88:2638–2649.

45. Schurch, S., F. H. Y. Green, and H. Bachofen. 1998. Formation and structure of surface films: captive bubble surfactometry. *Biochim. Biophys. Acta.* 1408:180–202.

46. Fenster, S. K., and A. C. Ugural. 2003. Advanced Strength and Applied Elasticity. Prentice Hall, NJ.

47. Gopal, A., and K. Y. C. Lee. 2001. Morphology and collapse transitions in binary phospholipid monolayers. *J. Phys. Chem. B.* 105:10348–10354.

48. Lipp, M. M., K. Y. C. Lee, D. Y. Takamoto, J. A. Zasadzinski, and A. J. Waring. 1998. Coexistence of buckled and flat monolayers. *Phys. Rev. Lett.* 81:1650–1653.

49. Manzanares, D., K. Rodriguez-Capote, S. Liu, T. Haines, Y. Ramos, L. Zhao, A. Doherty-Kirby, G. Lajoie, and F. Possmayer. 2007. Modification of tryptophan and methionine residues is implicated in the oxidative inactivation of surfactant protein-B (SP-B). *Biochemistry.* 46:5604–5615.

50. Nag, K., K. Rodriguez-Capote, A. K. Panda, L. Frederick, S. A. Hearn, N. O. Petersen, S. Schurch, and F. Possmayer. 2004. Disparate effects of two phosphatidylcholine binding proteins, C-reactive protein and surfactant protein A, on pulmonary surfactant structure and function. *Am. J. Physiol. Lung Cell. Mol. Physiol.* 287:L1145–L1153.

51. Gericke, A., C. R. Flach, and R. Mendelsohn. 1997. Structure and orientation of lung surfactant SP-C and L-α-dipalmitoylphosphatidylcholine in aqueous monolayers. *Biophys. J.* 73:492–499.

52. Johansson, J. 2001. Membrane properties and amyloid fibril formation of lung surfactant protein C. *Biochem. Soc. Trans.* 29:601–606.